Composites: Part A 155 (2022) 106825

Contents lists available at ScienceDirect

Composites Part A

journal homepage: www.elsevier.com/locate/compositesa

Experimental investigation of high strain-rate, large-scale crack bridging behaviour of z-pin reinforced tapered laminates

A.D. Cochrane [a], J. Serra [a], J.K. Lander [b], H. Böhm [c], T. Wollmann [c], A. Hornig [c], M. Gude [c], I.K. Partridge [a], S.R. Hallett [a,*]

[a] Bristol Composites Institute, University of Bristol, United Kingdom
[b] Rolls-Royce plc, United Kingdom
[c] Institute of Lightweight Engineering and Polymer Technology (ILK), Technische Universitat Dresden, Germany

ARTICLE INFO

Keywords:
3-Dimensional reinforcement
Laminates
Impact behaviour
Delamination

ABSTRACT

Significant research exists on small-scale, quasi-static failure behaviour of Z-pinned composite laminates. However, little work has been conducted on large-scale, high strain-rate behaviour of Z-pinned composites at structural level. Small-scale testing is often at an insufficient scale to invoke the full crack bridging effects of the Z-pins. Full-scale testing on real components involves large length scales, complex geometries and resulting failure mechanisms that make it difficult to identify the specific effect of Z-pins on the component failure behaviour. A novel cantilever soft body impact test has been developed which is of sufficient scale to invoke large-scale delamination, such that behaviour in Z-pin arrays at high strain-rates can be studied. Laminates containing Z-pin arrays were subjected to soft-body gelatine impact in high-speed light gas-gun tests. Detailed fractographic investigation was carried out to investigate the dynamic failure behaviour of Z-pins at the microscopic scale.

1. Introduction

Carbon-fibre reinforced polymers (CFRP) are increasingly being used in high-performance applications in order to provide weight savings while improving mechanical performance. Aircraft secondary structures such as spoilers and wing flaps, and now primary load-carrying lifting surface and engine structures are being designed and manufactured from CFRP [1]. The recent Boeing 787 commercial aircraft contains 50% composite materials by weight. Aerospace components are increasingly being manufactured using pre-impregnated carbon fibre sheets which build up a three-dimensional shape using two-dimensional layers, thus introducing vulnerability in the interlaminar region due to lack of fibrous material in the through-thickness direction [2]. These components have poor damage tolerance under impact conditions such as those encountered during bird-strike, with interlaminar crack formation known as delamination constituting a major failure mode, which may cause loss of component stiffness and strength and potentially catastrophic failure. Such behaviour has led to a large body of research into the improvement of the impact damage tolerance of composite structures such that delamination cracks are managed effectively and structural failure is avoided [3].

The problem of composites' impact damage tolerance may be partially resolved by enhancing the effective or apparent interlaminar fracture toughness of the resin layer between each ply. This may be achieved by several methods currently in mainstream use. One approach is to directly toughen the interlaminar resin layer through resin toughening by inclusion of particles made of e.g. thermoplastic or rubber to give improved damage tolerance characteristics in the inter-ply region. The particles act through mechanisms such as crack-blunting and crazing to aid in arresting crack propagation [3].

A more effective method for high-performance applications is to implement fibrous material in the through-thickness direction – most often at the preforming stage – and this practice is known as through-thickness reinforcement (TTR) [4]. The fibres inserted into the material act as micro-fasteners which mechanically inhibit crack propagation during fracture. By reinforcing the through-thickness direction, the composite becomes a 3-dimensional structure and large-scale cracks may only progress by pull-out or rupture of the reinforcing fibres depending on the nature of the loading conditions at failure. Several different through-thickness technologies are commonly used in aerospace such as tufting [5], stitching [6] and Z-pinning [7], with the latter being the primary technology employed in structures manufactured from pre-preg and the focus of the current study. Z-pins were first conceived by the US company Foster-Miller Inc. in the 1980s [8]

* Corresponding author.
E-mail address: stephen.hallett@bristol.ac.uk (S.R. Hallett).

https://doi.org/10.1016/j.compositesa.2022.106825
Received 1 October 2021; Received in revised form 21 December 2021; Accepted 12 January 2022
Available online 29 January 2022

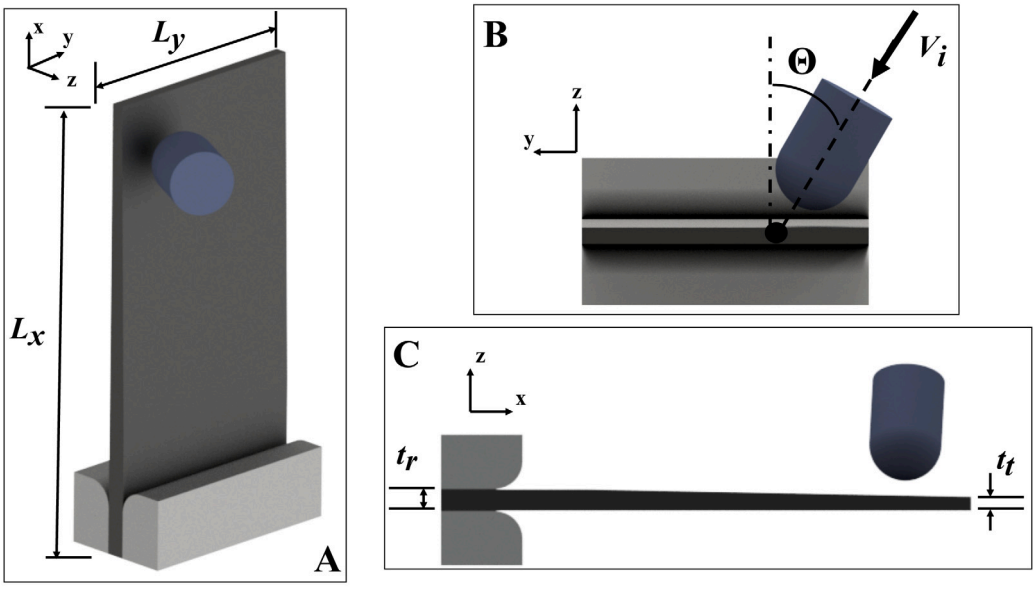

L_x [mm]	L_y [mm]	t_r/t_t	t_r [mm]	V_i [m/s]	Θ [°]	(p_x, p_y) [mm, mm]	d_i [mm]	l_i [mm]	m_i [g]
290	180	3/2	12	165	15	(270,20)	40	60	71

Fig. 1. (Top) Isometric (A), viewed along *x*-axis (B) and viewed along *y*-axis schematic representations of the impact test configuration; (bottom) the numeric values for key parameters associated with the test design.

and have been employed in a range of applications since. The pins are thin pultruded rods consisting of bundles of continuous fibres and resin, which are inserted in predefined arrays by various means into uncured laminates at the preforming stage [9]. They are generally made from carbon-fibre material, but have also been produced using metallic materials [10].

The effectiveness of Z-pins in providing enhanced interlaminar fracture toughness has been extensively researched in literature, with the majority of work focussing on testing at small-scale coupon level and quasi-static strain rates. A variety of loading cases have been considered. Some dynamic testing has been conducted at coupon level at high strain-rates, with results showing similar trends to quasi-static testing in terms of pinned fracture toughness mechanisms and improvements [11–14]. At higher strain-rates, generally the failure becomes more 'abrupt', which can affect the total energy dissipated during failure. While these test campaigns have demonstrated the effectiveness of single pins and small arrays of pins at coupon level and a range of strain rates, it has been shown that the effectiveness of Z-pins at arresting crack propagation cannot be fully realised until the pins undergo large-scale interlaminar crack bridging [7,15–17]. In this scenario, a crack of sufficient length is developed such that multiple rows of pins are traversed by the crack as it propagates, causing the pins to 'bridge' the fracture surfaces. When this large-scale bridging occurs, the maximum possible apparent fracture energy is generated by the pins to retard further crack propagation. At the commonly used smaller test scales, this behaviour is not possible.

A bespoke test design, the soft-body beam bending (SBBB) method, was developed for use with Z-pinned composite specimens [18] to investigate their crack bridging behaviour. The method generated a Mode-II dominated crack at the mid-plane of the laminate, with the mode-ratio estimated by fractographic investigation and high-speed video analysis. As the crack propagation was essentially 1-dimensional and the mode II crack opening was limited by the scale of the specimen, it was desirable to extend this approach to investigate Z-pin bridging behaviour at larger length scales and under more diverse loading conditions. A novel test, which created large-scale delamination behaviour, more representative of that seen in real component failure [19], provides a laminate geometry large enough to allow multiple Z-pin arrays to be included and undergo full-scale crack-bridging. This test provides a platform for the current investigation of Z-pin behaviour under a range of loading conditions, with the dimensions of the specimen allowing for experiments involving large length scales and structural interactions. The test involved the impact of a tapered laminate using a soft-body gelatine projectile under impact conditions that were tuned to generate a large, single delamination crack near the laminate mid-plane. Fractographic investigation showed a highly Mode II crack, with indications of a change in the crack mode-ratio during propagation. The work in [19] demonstrated crack development in an unpinned laminate, the current study considers laminates reinforced with Z-pins.

The test specimen geometry, boundary conditions and key test parameters are summarised in Fig. 1. This test provides the means to fill a significant gap in the aerospace certification pyramid of testing for a structural sub-element scale test. The purpose of this work is first to demonstrate the validity of this test for assessment of through-thickness reinforcement technologies, and second is to investigate in more detail the failure behaviour of Z-pins under representative loading conditions, to assist in informing future attempts to capture this behaviour in models. This large-scale bridging behaviour of Z-pins under high strain-rate conditions and their effect on fracture morphology observed in the component was therefore investigated through SEM fractography on the fracture surfaces of failed specimens containing pins.

2. Z-pin configuration design

This study aims to demonstrate the behaviour of Z-pins encountering a large-scale, high strain-rate delamination failure scenario. The test method developed in [19] successfully produced a large and highly Mode II crack predominantly on a single interface in a tapered, cantilevered laminate. Within the confines of this test configuration, the

current study aimed to arrest the developed crack using arrays of inserted Z-pins. Based on the results for an unpinned specimen obtained in [19], the Z-pin array configuration was designed to arrest a high-energy, highly Mode II crack. For the purposes of this study, the 'baseline' pin architecture of normally-aligned carbon fibre (*NACF*) was used. In-line with common practice in the aerospace industry and for manufacture using existing equipment, the areal density of pin arrays was fixed at 2%.

In prior work [20], it was shown that for *NACF* Z-pins, pin length did not have a significant effect on the interfacial fracture toughness in a Mode II delamination scenario i.e. in predominantly shearing/sliding failure. In this failure mode, any pull-out action was largely suppressed and pins failed by shear rupture. Shear rupture is generally governed by the transverse shear strength of the pin, which for *NACF* Z-pins is low. Improvements in Mode II fracture resistance have generally been achieved through increasing the number of *NACF* pins which encounter the crack front, thus increasing the total pin cross-section area providing shear resistance [17]. Much greater Mode II improvements have been generated if the pin material was changed to a more ductile material such as a metal [10]. Changes to the pin insertion angle – depending on the load configuration – have also improved Mode II fracture resistance by shifting the failure mode from shear rupture to pull-out, thus invoking energy dissipation by frictional resistance [21]. However, if the pin architecture and pattern is constrained to *NACF* pins arranged at 2% areal density (as in this case), then the only way to improve shear resistance is to enlarge the pin arrays themselves, i.e. to insert more pins.

It was demonstrated in [19] that the delamination crack generated in an unpinned specimen initiated near the root and travelled lengthwise towards the tip. This crack was seen to be primarily Mode II through fractographic analysis. Any designed Z-pin array configuration would therefore aim to place as many Z-pins as possible between the root and tip to successfully arrest the Mode II crack as it propagated. However, due to a reduction in local laminate strength in regions where they are inserted, Z-pins can introduce vulnerability into the structure [9]. This had to be taken into account when designing for the insertion of large numbers of pins to avoid unwanted fibre failure.

The pin configuration was proposed to be made up of chordwise bands of pins which extended across the majority of the specimen width but with a 7 mm gap between the edge of the band and the laminate boundary (Fig. 2(a)), placing a large number of pins in the crack propagation path. Gaps were left at the edges to allow for some continuous and undisturbed fibres to extend from the root to the tip and prevent introducing an entire region of vulnerability across the chord. Two 19 mm-wide bands of pins were used, with the first band – closest to the tip – placed approximately at the mid-span, and the second band placed closer to the root with a bandwidth (less one row of pins) between them. The dimensions of the arrays were such that they contained 12×72 pins at 2% areal density. This was defined as the *2-Row* or *2R* pattern. In order to assess the effect of increasing the number of pins, and of placing consecutive bands of pins in the crack path which could dissipate crack propagation energy sequentially, another pattern type was designed which included an extra band of pins closer to the root. This was defined as the *3-Row* or *3R* pattern (Fig. 2(b)). The *2R* pattern represented a 12.4% pinned area of total planform area, while the *3R* pattern represented 18.6%. The two different patterns were used to examine the enhancement in damage tolerance provided in terms of increasing number of pins, arranged in similar banded patterns.

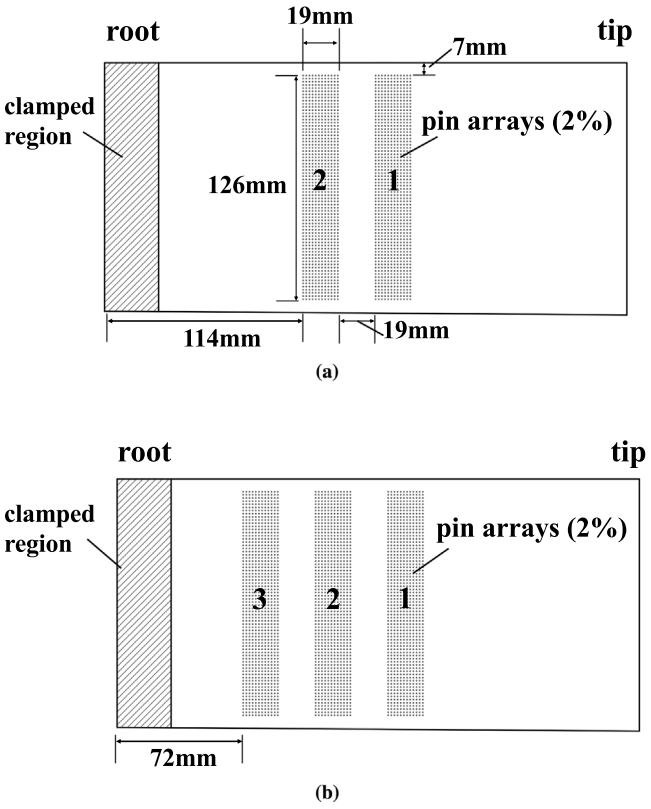

Fig. 2. Top-down view of the designed pin patterns with pin rows annotated with the relevant row number, where (a) shows the *2R* pin pattern made up of two chordwise rows (*Row 1* and *Row 2*), and (b) shows the *3R* pattern where an extra identical chordwise row (*Row 3*) has been inserted close to the root region. The highlighted clamped region is where the fixture comes into contact with the laminate.

3. Manufacture & testing

3.1. Specimen manufacture

Six tapered specimens were manufactured from sheets of Hexcel UD IM7/8552 pre-impregnated carbon fibre material using hand lay-up to form a bespoke 0-degree dominated laminate, also featuring +45, −45 and 90-degree plies. See [19] for details, which also include information on the ply drop sequence used to achieve the laminate tapering. A single 2 × 2 plain weave M21/IMA prepreg sheet was added to both the upper and lower surfaces to protect the underlying UD plies from impact damage and contact stresses near the fixture. The Z-pins had a diameter of 0.28 mm and were manufactured from T300/BMI material. Pinning was performed after layup and prior to curing. Unpinned specimen preforms were manufactured using the method outlined in [19], where silicone sheeting was placed above and below the laminate to act as a pressure intensifier and to protect the tool-plate beneath and vacuum bag above from protruding Z- pins during consolidation (see Fig. 3). The pins were inserted such that they spanned the entire depth of the laminate and no unpinned thickness remained. This was achieved by inserting pins with excess length, then shearing off the excess pin length with a blunt blade. The specimens were linearly tapered for a portion from the root to the tip over a length of 260 mm. This shallow taper meant that pins within each array reduced in length from the root towards the tip, and in each array the effective pin length was shorter than those arrays closer to the root. A standard IM7/8552 aerospace cure cycle was applied to the preforms [22].

3.2. Experimental setup & test method

Gelatine impact testing of the Z-pinned laminates was conducted to investigate the through-thickness reinforced delamination performance compared to the unpinned laminates tested in [19] and investigate the dynamic large-scale crack-bridging behaviour of the Z-pins. Testing was conducted using a light gas-gun apparatus with the parameters such as

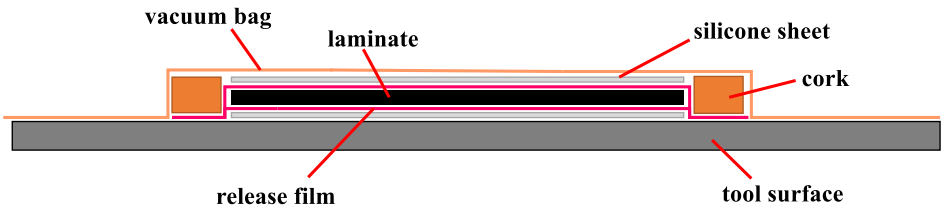

Fig. 3. Schematic diagram of the vacuum-bagging configuration for each laminate, showing use of 3 mm silicone sheeting between the upper laminate surface and the vacuum bag, and lower laminate surfaces and tool-plate, in order to prevent damage to the vacuum-bag or tool-plate by protruding pins during consolidation.

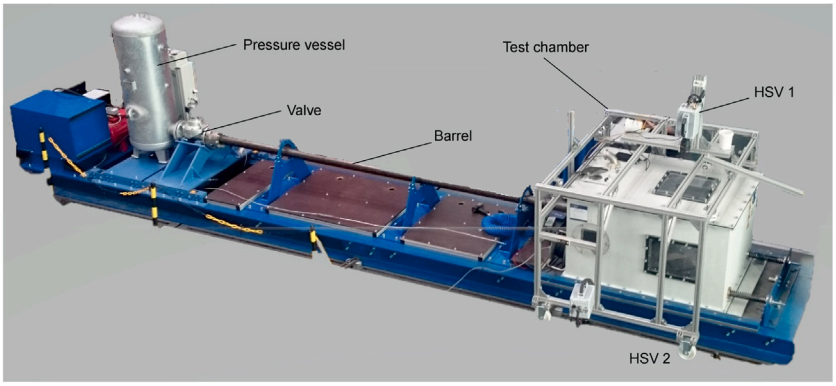

Fig. 4. Photograph of gas-gun system.

projectile impact velocity, incidence angle and location developed and validated in [19]. The test fixture is shown in Fig. 1 and the gas-gun apparatus is shown in Fig. 4. A 60 mm long gelatine shot of 40 mm diameter and with a 20 mm radius hemisphere at the forward end was fired at an initial velocity of $V_i = 165$ m/s and incidence angle of 15° at a laminate clamped between two fixture plates using bolts tightened to a pre-defined torque. The gelatine was made via an aqueous solution of powdered ballistic gelatine and water mixed in a pre-defined ratio. The sabot was manufactured from polyurethane foam inside a closed mould and sanded and greased by hand prior to firing. It was then rammed to the end of the barrel to its firing position. The entire test fixture was located within an impact-resistant metallic chamber which contained transparent plastic windows to allow for viewing and high-speed camera recording of the impact event. The pressure vessel was pressurised to a prescribed value based on prior calibration in order to generate the correct projectile velocity on firing.

Two high-speed video (*HSV*) cameras running at 25,000fps were used to record laminate displacements, projectile velocity and crack propagation. The *HSVs* were placed orthogonal to the short tip-face of the laminate (*HSV1*) and orthogonal to the long edge furthest from impact (*HSV2*) as shown by Fig. 5. Each laminate was marked up by a series of lines and dots, consistent with the method in [19], to allow displacement and crack propagation tracking. A solvent-based alkyd paint was used for the white coating.

The tests were conducted on six pinned laminates: three containing Z-pins in the *2R* configuration and three containing pins in the *3R* configuration, as outlined in Section 2. The ability of the test method to reliably produce a single, large delamination near the mid-plane was validated through the unpinned testing in [19], so the focus of this paper is on the behaviour of the Z-pinned laminates relative to those containing no pins and the effects on laminate failure behaviour. For all pinned laminates, the extent of delamination was measured using ultrasonic C-scanning. C-scanning was also performed before each test to verify the integrity of each laminate. The through-thickness location of delamination was observed by viewing crack edge propagation both in the high-speed video (HSV) footage and visually after testing. Specimen and gelatine dynamic behaviour were observed using both HSVs. Tip deflections were measured by postprocessing *HSV1*, but measurements were generally corroborated with those from *HSV2*.

3.3. Results

The individual test parameters and results are summarised in Table 1. Average root thickness was $t_r = 12.58$ mm (4.8% over nominal) and tip thickness was $t_t = 9.05$ mm (13.8% over nominal). The average gelatine mass was 71.8g, which is approximately 15% over the nominal design mass. For the tuned test configuration from the unpinned tests, the nominal impact velocity was fixed at $V_i = 165$ m/s to generate a large amount of delamination. Delamination initiates from the root region and travels lengthwise towards the tip, with pins placed in the assumed region of crack front propagation, as described in Section 2. For all pinned tests, specimens showed an average of delamination area, $A_d = 56\%$ ($CoV = 0.0923$). This result had a high degree of repeatability across all tests in terms of dynamic response and failure. Test parameters were maintained within acceptable tolerances, e.g. test speed was within ±2.5 m/s of the target speed.

3.4. Experimental observations

3.4.1. Impact response

Analysis of the specimen dynamic response, particularly in terms of deflections and their relation to crack propagation, was performed through examination of the HSV footage. Very similar general dynamic behaviour was observed as for the unpinned specimens tested at $V_i = 165$ m/s in [19]. The initiation of delamination appears unchanged by the presence of the through-thickness reinforcement, as would be expected, with initiation taking place near the root. It is assumed that the exact point of initiation is on the opposite side of the chord to impact and at the root where the laminate is gripped by the fixture, due to this being the location of maximum bending/shearing based on the applied impact loading. Similarly to the unpinned case, the specimen undergoes

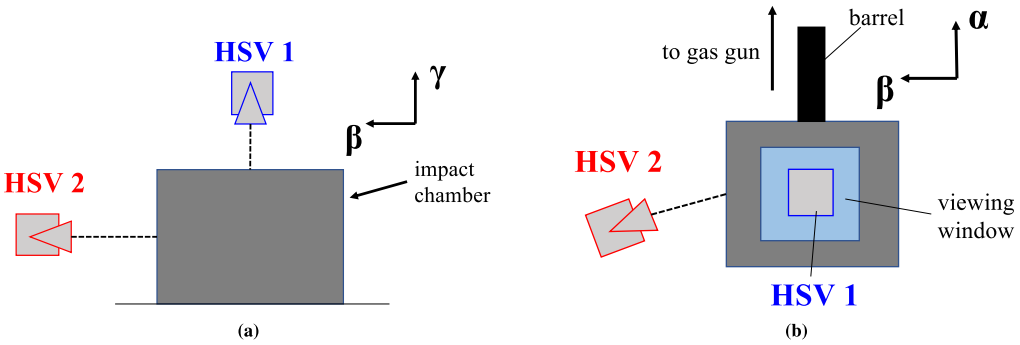

Fig. 5. (a) Schematic diagram of high-speed video camera (HSV) configuration viewed along gas-gun α-axis, showing *HSV1* above impact chamber pointing vertically downwards (in γ−direction) and *HSV2* pointed orthogonally at the long edge of the specimen (b) rotated version of diagram (a) viewed along the gas-gun γ-axis.

Table 1
Results for the pinned gelatine impact tests.

Specimen ID	Tip thickness [mm]	Root thickness [mm]	Gelatine mass [g]	Velocity [m/s]	Impact Energy [J]	A_d [%]
2R1	9.1	12.8	71.2	165	969.2	62
2R2	9.0	12.5	71.8	163	954.1	57
2R3	9.2	12.6	71.6	165	975.1	48
3R1	9.0	12.4	72.2	164.4	975.1	61
3R2	9.2	12.4	71.9	167.2	1004.3	55
3R3	9.1	12.7	71.9	164.3	970.2	54

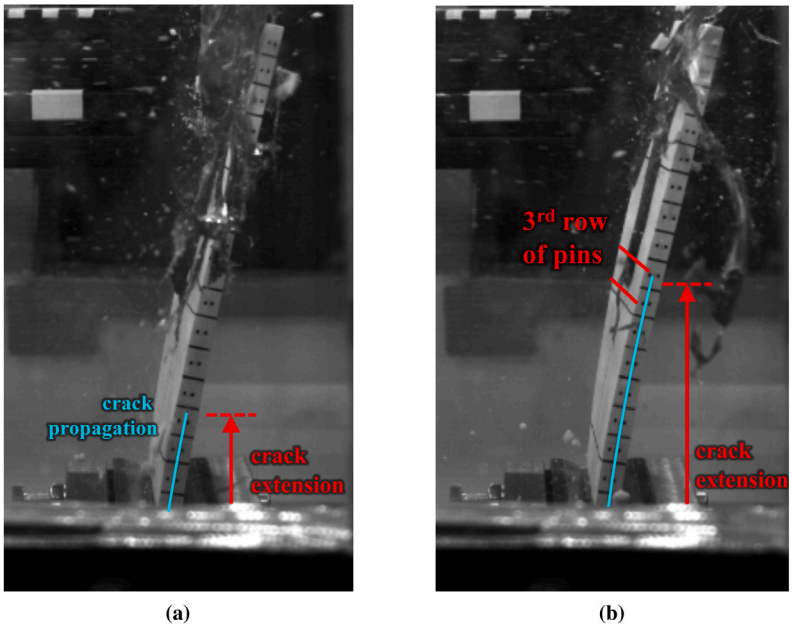

Fig. 6. Illustration of the crack propagation viewed from *HSV2* along the long edge during test 3R1, showing location of crack arrest roughly corresponding to the location of the 3rd row of pins along the span (*Row 1* in Fig. 2); (a) shows the initial crack propagation after impact, while (b) shows the moment when the crack stops moving along the visible edge.

a large twisting deflection on the side of impact followed immediately by a reversed twisting deflection; these deflections occur during an overall initial downwards longitudinal bending deflection. It appears that delamination initiates at some point during these initial large deflections, and the crack quickly propagates during the bending reversal. For the specimens containing z-pins, crack propagation appears to be arrested around the mid-span of the laminate in each case (Fig. 6). This result is consistent across all tests, both for specimens containing the *2R* pin pattern and the *3R* pin pattern. Gelatine behaviour is very similar across both unpinned and pinned tests. The gelatine appears to deform substantially on initial impact but remains largely a single, solid mass — it then moves across the width of the specimen as it undergoes twisting before departing the laminate surface. The ultimate extent of crack propagation along the visible specimen edge is shown on an impacted pinned 3R specimen in Fig. 7.

3.4.2. Deflection measurements

Due to a high-speed video camera *HSV1* failure during tests *2R1* and *2R3*, these tests are omitted from tip displacement measurement analyses. Fig. 8 identifies the location of the displacement measurement points in the *HSV* footage. Fig. 9(a) shows the tip displacement as measured from the location *S1* through *HSV1*, where tip displacement

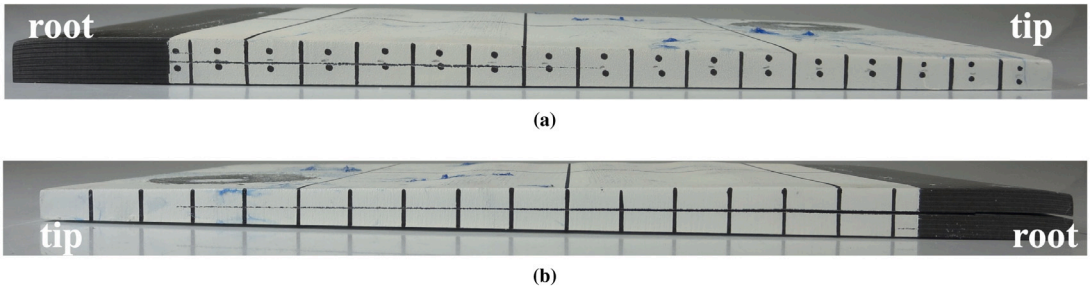

Fig. 7. Post-impact photograph of the long edges of specimen 3R1, showing final crack arrest location, with (a) the side visible in *HSV2* and in Fig. 6, and (b) the side closest to the gas-gun.

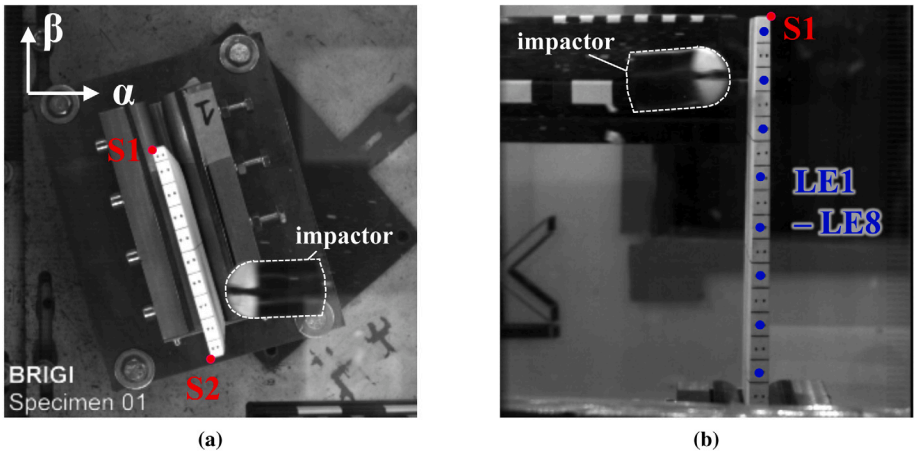

Fig. 8. (a) Still from *HSV1* showing displacement measurement points *S1* and *S2*; (b) Still from *HSV2* showing displacement measurement points *S1* and *LE1-LE8*.

in this case is the displacement along the gas-gun α-axis of the given point. Fig. 9(b) shows the averaged tip *S1* displacement for the unpinned (*U/P*), 2-row (*2R*) and 3-row (*3R*) reinforcement configurations at V_i = 165 m/s, showing the similarity in tip displacements across all results. Fig. 10(a) and Fig. 10(b) show surface plots of the beam bending measured at the spanwise locations *LE1 - LE8* in Fig. 8, both at an experiment time of 10 ms after impact occurs. Fig. 11 shows the experimental twist results for the pinned cases, and a comparison between the averaged unpinned and pinned twist. There is not a significant change in the deflection results between tests. A peak negative α-axis displacement of approximately $d_\alpha = -60$ mm is observed at location *S1*. From Fig. 10(a) and Fig. 10(b), the beam bending response is very similar across all tests. It can be seen from both the tip displacements and beam bending results that very similar responses are obtained for all laminates at V_i = 165 m/s. The corresponding C-scans for all pinned results are given in Fig. 12. A similar delamination profile is observed across all pinned tests.

This observation helps to illustrate the fact that the deflections are highly dependent on the delamination condition of the laminate, as was observed in [19], but not necessarily on the exact test parameters used. In [19] it was observed that large differences in delaminated area can cause large differences in the maximum observed tip deflections. Contrarily the pinned results, which are broadly consistent in terms of the delaminated area, show very little difference in the tip deflection response.

3.4.3. Delamination

No evidence of any delamination was detected prior to each test in the Z-pinned laminates by the ultrasonic C-scans. In each of the pinned cases, the delamination is clearly arrested by the Z-pins across a large portion of the specimen width. There is evidence of both delamination travelling through the pins, on the closest side to impact, and of being arrested on the side farthest from impact. In each case, the projected delamination pattern was measured via ultrasonic C-scan and these are shown in Fig. 12. The cause of the delamination extending farther lengthwise on one side than on the other is most likely due to the way the specimens twist after impact (Fig. 11), which is a function of the stiffnesses and thus the layup, and also the layout of the pin arrays. This difference in propagation along each edge is also present in the unpinned specimens, suggesting that it might be possible to control it by altering the laminate stiffness. These results imply that a combination of laminate design and pin arrangement will allow for the deflections to occur in such a way that the delamination is channelled into the pins favourably and arrested effectively.

The layout of the pins in rows and the lengthwise propagation of delamination allows for observation of the effect of each successive row of pins and testing of the theory that pins act as 'crash bands', sequentially removing energy from the propagating crack and diverting delamination away from key structural areas — demonstrating *delamination management* capability. For both the *2R* and *3R* cases, the final delamination profile – in terms of where propagation stops and overall delamination area reduction – is very similar. Given that the *3R* pattern contains an extra array of pins closer to the root than *Row 1* and *Row 2*, the fact that the delamination is largely unchanged suggests this extra array does not assist in arresting crack propagation. This result suggests that placement of *Row 3* may be too close to the location of initiation, which indicates that placement of arrays of pins relative to the predicted crack path is important in determining their effect on delamination suppression.

Fig. 13(a) shows the delamination area A_d – calculated using A_d = (delaminated area/total specimen area) – obtained via C-scan post-processing. The delaminated area is quite consistent across all tests, with an average of 56% of the primary interface delaminated. Contrary to the unpinned specimen delamination results summarised in [19],

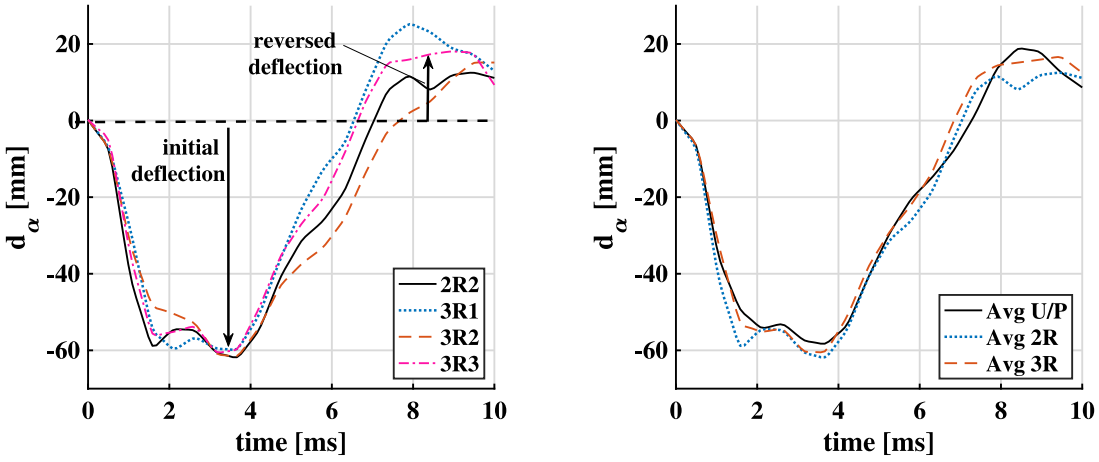

Fig. 9. (a) tip displacements from tests *2R2, 3R1, 3R2* and *3R3* on pinned laminates showing data taken from point *S1*; (b) averaged unpinned (*U/P*), 2-row (*2R*) and 3-row (*3R*) tip displacement results from the same location.

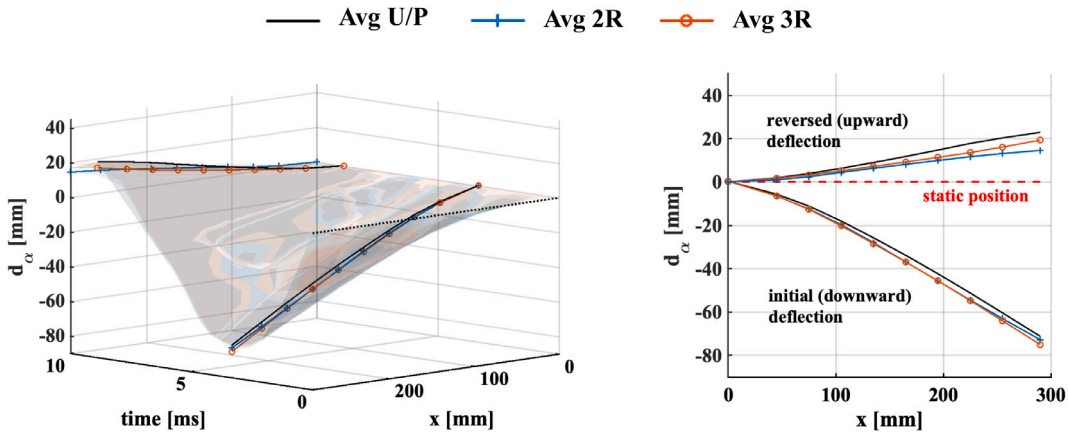

(a) Isometric view showing variation of displacements in time

(b) Profile view showing maximum and minimum beam deflection points only

Fig. 10. Variation in the α-axis displacement of each point *LE1 - LE8* along the span using averaged displacements across each laminate configuration (unpinned (*U/P*), 2-row (*2R*) or 3-row (*3R*)), with (a) illustrating the variation in the beam displacements over time with the minima and maxima highlighted, and (b) showing a side-on profile view of the minimum and maximum displacements across all points in time.

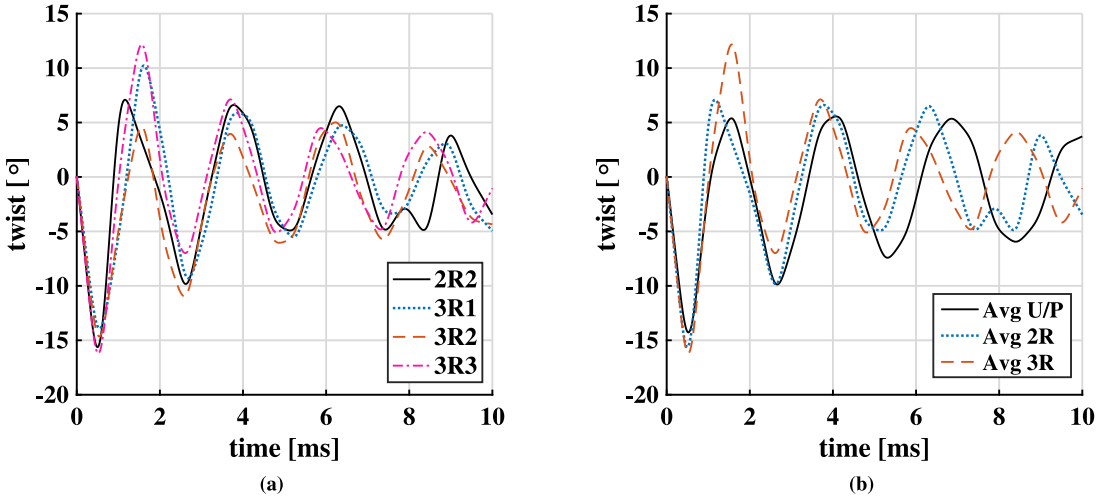

Fig. 11. Specimen twist extracted from the difference in tip displacements from points *S1* and *S2*, with twist being taken as + ve anti-clockwise when viewed along the specimen *x*-axis from tip to root. (a) shows the twist values for each individual pinned test (*2R2, 3R1, 3R2* and *3R3*); (b) shows the twist values averaged across each laminate configuration (unpinned (*U/P*), 2-row (*2R*) or 3-row (*3R*))

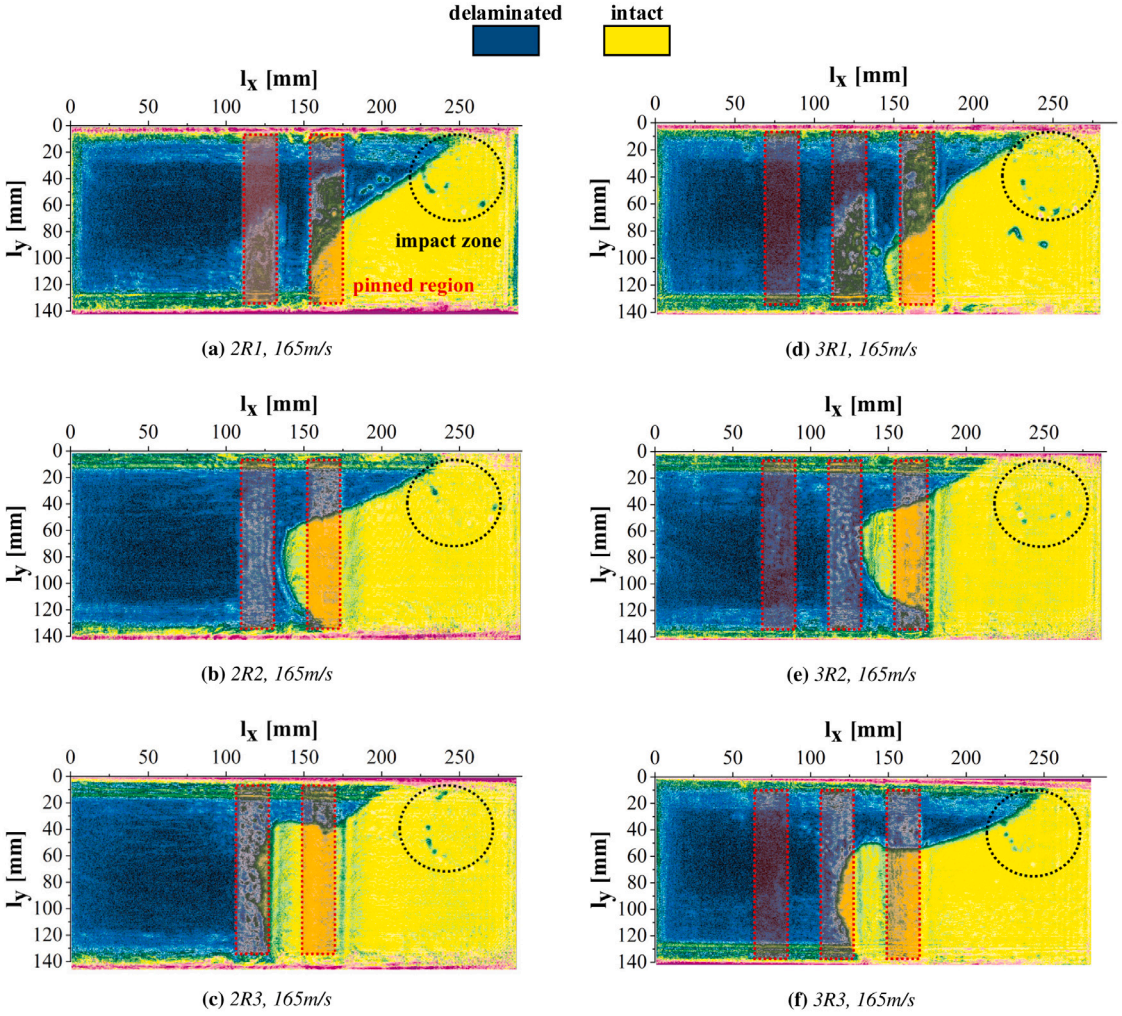

Fig. 12. C-scan plots of delamination across the full specimen area for pinned laminates *2R1 - 3R3*, showing region of impact and pinned areas. The specimen root corresponds to $l_x = 0$ mm, the visible edge in *HSV1* corresponds to $l_x = 290$ mm and the visible edge in HSV2 corresponds to $l_y = 140$ mm.

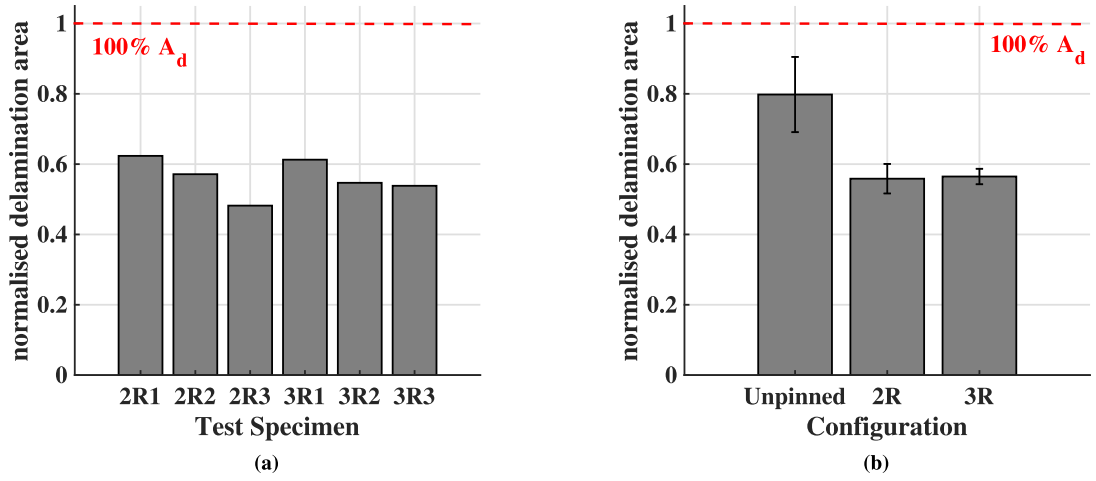

Fig. 13. (a) normalised delamination area computed as the delaminated area A_d as a fraction of the specimen in-plane area for the unpinned tests *2R1 - 3R3*; (b) Averaged normalised delamination area A_d for the unpinned (*U/P*), 2-row (*2R*) and 3-row (*3R*) configurations.

there appears to be far less sensitivity of the delamination to even very small changes in the environment or test parameters. For an unpinned laminate in the same nominal test configuration, the delamination result varies between 64 – 100% delaminated area A_d, while the pinned specimens show variation between 48 – 62%. This shows that inclusion of pins in a structure may reduce failure result variability in an impact

scenario to one that is more predictable and stable in terms of crack propagation.

Fig. 13(b) shows the average normalised delamination area results achieved for unpinned, *2R* and *3R* laminates. A reduction to the equivalent unpinned delaminated area is achieved for those specimens pinned in a *2R* pattern, while no significant improvement is observed when the specimens contain an extra row of pins. This result indicates that inclusion of a greater number of pins is not necessarily conducive to a reduction in damage or an improvement in damage tolerance. The use of Z-pins introduces mechanical property knock-downs [9], and so this result highlights that they should only be inserted when it they will have an effect on crack propagation. Further work is required to investigate the reasons for the ineffectiveness of the third row of pins.

Overall, the pinned laminates therefore give an average reduction in delaminated area of 24%. However, increasing the number of pins from 1,728 in the *2R* pattern by 50% to 2,592 in the *3R* pattern does not yield any further reduction in delaminated area. Furthermore, the addition of 864 extra pins is not insignificant in terms of affecting the substrate quality and time necessary for manufacturing. Additionally, the proportions of total laminate in-plane area with pins inserted – 12.4% for the *2R* specimen, and 18.4% for the *3R* specimen – are very significant. In practice, inserting Z-pins into an aerospace load-carrying composite component with Z-pins in these proportions could lead to significant laminate property knock-downs, and should generally be avoided. However, the large number of Z-pins required to arrest the crack in the high-energy impact scenario presented may be attributed to the relative poor mode II performance of *NACF* pins inserted into pre-preg material; as described in Section 2 this pin type has a low transverse shear strength, the governing property for a normally-aligned Z-pin loaded almost purely in shear. Using a material with greater mode II effectiveness – such as a metal – may result in the same performance but with a reduced number of pins. Use of a prescribed insertion angle, loaded 'with the nap' [21] i.e. in-line with the load vector – may shift the failure mode to pull-out rather than shear, allowing carbon-fibre pins to be used much more effectively but with the limitation that the loading configuration must be known, and manufacturing would require specialist equipment.

The experimental test programme conducted here has generated high-level understanding of the way the arrays of Z-pins interact with the delamination crack, but more detailed understanding is desired on the failure mechanisms involved. In the current test results, it is likely that the crack mode-ratio at failure is not purely Mode II but mixed-mode in nature. Examination of the *HSV2* footage suggests that some crack-opening occurs during crack propagation, especially on the reversed longitudinal bending return stroke after the initial impact. In order to more closely investigate the failure behaviour of both the unpinned and pinned interfaces, an SEM fractography investigation was carried out to determine the nature of the Z-pin failure on a microscopic level.

4. SEM fractography

In [19], the fracture behaviour of an unpinned (*U/P*) specimen – defined as specimen A – was investigated at the micro-scale through a detailed fractographic investigation. In this study, a *2R* pinned and *3R* pinned specimen – *2R1* and *3R1*, termed as specimens B and C respectively – were subjected to a similar investigation to generate understanding of pin failure behaviour. A number of fracture regions across the entire crack surface area, each with an upper and lower fracture surface, were selected from each plate and are identified in Fig. 14. The orientation of the *upper* and *lower* fracture surfaces relative to the overall plate geometry, for the purposes of this analysis, is outlined in Fig. 15.

For each fracture region, both the upper and lower surfaces were examined using a tabletop Hitachi T3030 scanning electron microscope. For the Z-pinned regions, lower-magnification images (20 – 300×) were

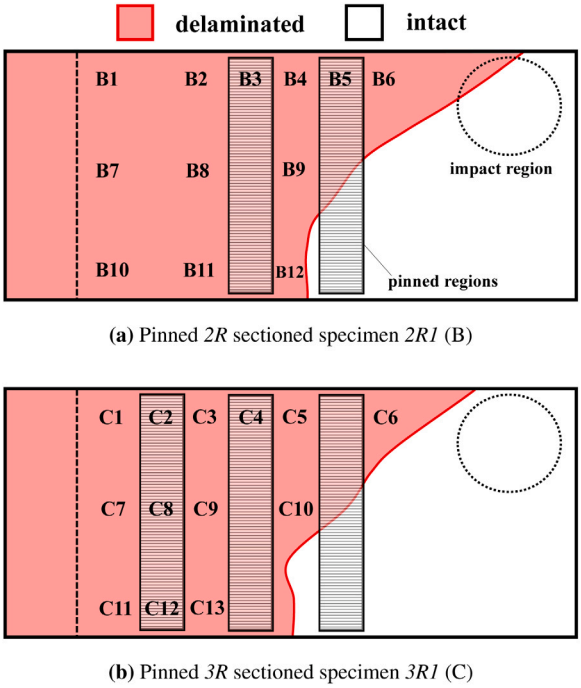

(a) Pinned *2R* sectioned specimen *2R1* (B)

(b) Pinned *3R* sectioned specimen *3R1* (C)

Fig. 14. Fracture diagrams illustrating the cracked region, shown in *red*, overlaid on the specimen geometry with regions e.g. *B1* selected for fracture analysis indicated. The pinned regions are indicated, along with the impact location and clamped root region.

taken of the failed pins where pins had fully sheared, allowing the two fracture surfaces to be separated. The investigation sought to determine Z-pin failure behaviour in more detail by examining features specific to the Z-pinned fracture regions.

4.1. Pin failure mechanisms

Where sheared pinned regions were examined, several types of failed pin features were observed. In many cases, the pins protrude from one fracture surface – indicating a non-pure Mode II failure – and the opposing surface contains a hole where this protruding pin section has been pulled out or a length of pin has been destroyed (Fig. 16). There is also clear evidence of *ploughing* of the pins into the surrounding laminate substrate, where the pin is forcefully pushed into the matrix resin via shearing (Fig. 17(a)) [23]. Multi-direction ploughing is suggested from many of the deformed resin regions surrounding pin holes. In many cases, the pin has been seemingly been pulled in two or several directions during fracture. A possible reason for this is that a pin is initially ploughed into the resin in one direction before rupturing, then it is pulled in the reverse direction by the interaction between the opposing fracture surface and the loose pin end. It often appears that during shearing of the pin, fibres have been 'gouged' from below the fracture surface (Fig. 17(b)). This results in a highly complex damaged fibre architecture surrounding many of the pin holes and one which appears to have been created in a particularly violent, high-energy fracture event.

Other evidence of energy dissipation mechanisms are fibre dragging, where it appears that the protruding pin ends have been 'dragged' along the fracture surfaces and caused damage (Fig. 18). This is evident by both the damaged fibres which appear to be stuck behind the protruding pin ends — and apparent 'smoothing' of the pin ends, as though 'ground down' via abrasion. In many cases, there is matrix debris surrounding the pins, indicating abrasion during shearing. In cases where dragged fibres are present on one surface, regions of removed fibres may be found on the opposing surface.

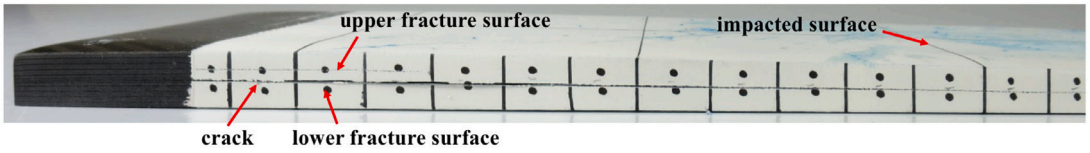

Fig. 15. Location of the *upper* and *lower* fracture surfaces described throughout this investigation as indicated on an impacted specimen.

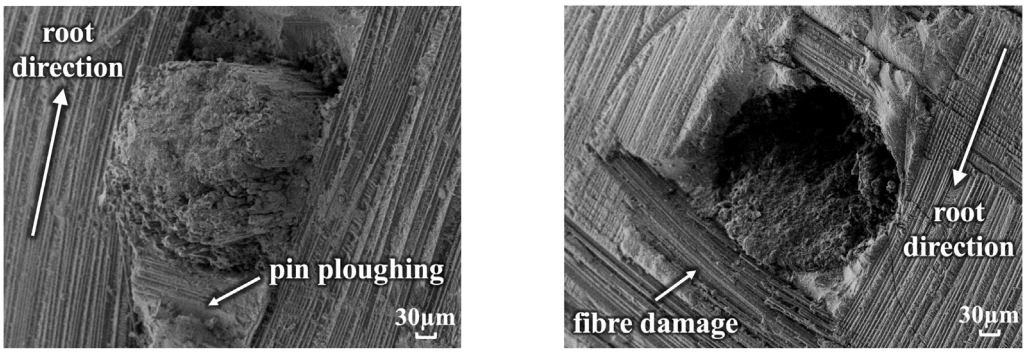

Fig. 16. (a) shows an SEM micrograph (250×) from the lower surface of region *C4* showing pin-end protrusion from the fracture surface, and (b) shows a cavity from the upper surface of the same region where a protruding pin has been pulled from the hole along with associated debris (250×). Subsequent images share the same indicated root directions for the lower and upper fracture surfaces.

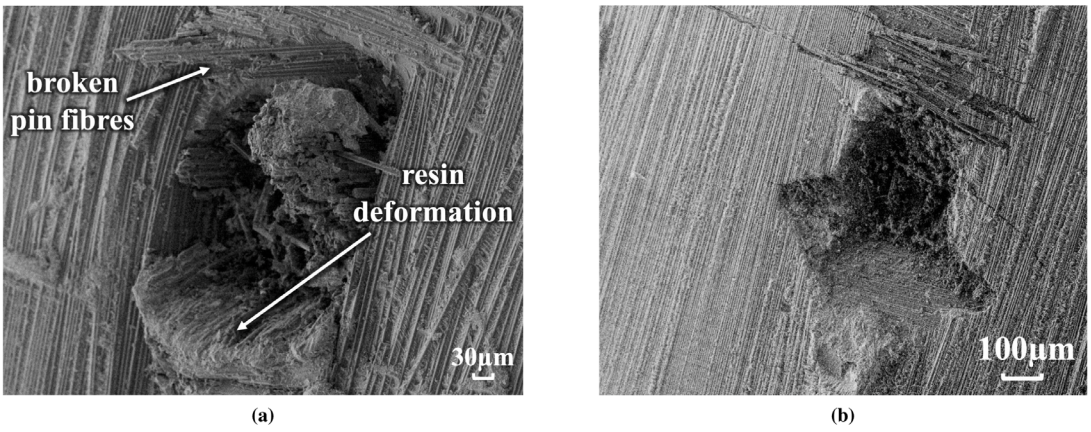

Fig. 17. (a) SEM micrograph from lower surface of fracture region *C4* showing clear evidence of resin deformation due to pin ploughing as well as residual pin fibres left protruding from the cavity after failure (250×); (b) Upper fracture surface of region *C8* showing significant substrate damage surrounding a pin hole containing pin and laminate debris (100×).

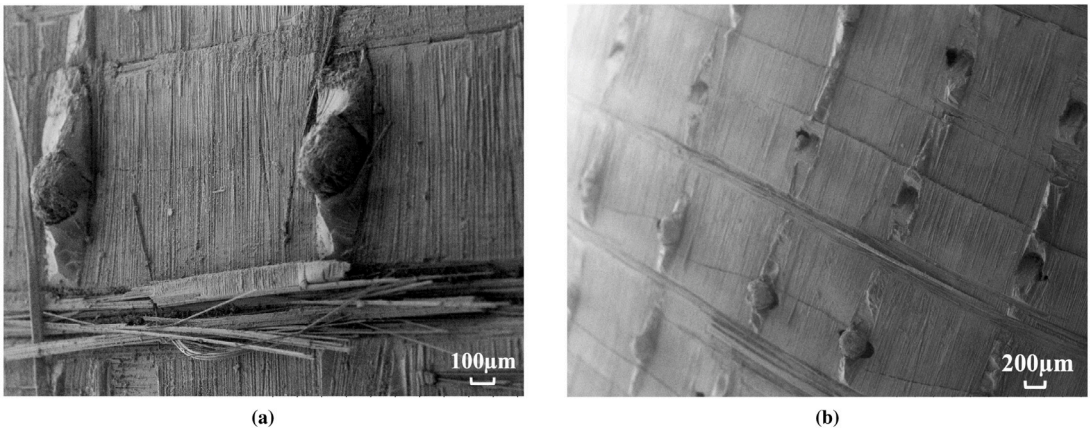

Fig. 18. (a) Evidence of fibre dragging on the upper fracture surface of region *C4*, as well as protruding abraded pin ends and deformed resin eyelets around pins (80×); (b) Low-magnification (30×) view of the type of fibre damage shown in 18(a), showing large regions of apparent dragged fibres and transverse fibre damage.

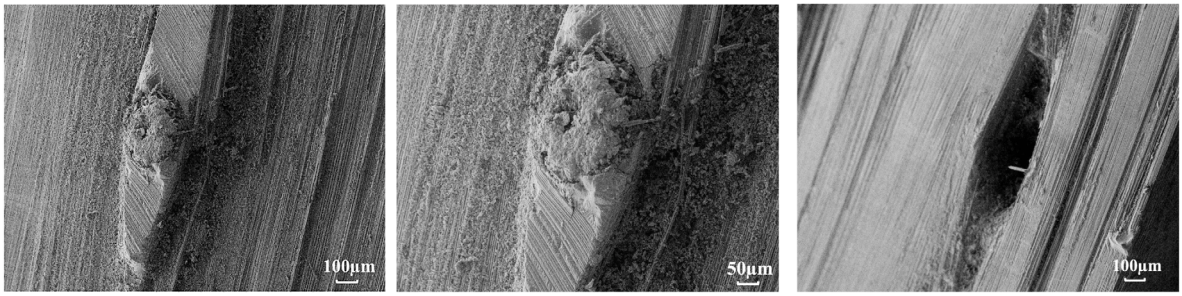

Fig. 19. (a) *Resin island* surrounding a shallowly-protruding pin-end on the upper surface of region *C8*, showing abraded pin tip and 45° fibre-imprints across the surface of the island (100×); (b) Closer-in view of the protruding pin-tip in (a) showing tip abrasion and island surface detail (180×)' (c) Large *substrate divot* from the fibre-dominated lower surface of region *C8*, showing a region where much of the substrate has been gouged by the violent delamination and where a large amount of the material comprising the pin eyelet has been removed to the opposing fracture surface (100×)

Resin islands are also present around some pins (Fig. 19) and areas of resin appear to have been removed around some pins. Each resin island is generally surrounding a protruding pin end. The fact that resin has been 'lifted' from one of the fracture surfaces — leaving a deep 'substrate divot' on the opposing surface (Fig. 19(c)) further suggests some form of opening mechanism. Pure shearing would likely not allow for such three-dimensional resin features on the fracture surfaces. This type of feature also reinforces the idea that significant amounts of energy have been dissipated by mechanisms not previously observed, possibly due to a combination of the very high strain-rates experienced and the mixed-mode crack which sees multiple different loading configurations as it develops.

Not all fracture surfaces could be observed, as in some cases, although the laminate had fractured, the sectioned pieces could not be separated. In these cases it was assumed that the z-pins were at least partially intact, but had been successful in slowing or halting the delamination progression. Fig. 20 shows the maps of the 2 and 3 row specimens, indicating the locations of fully and partially failed z-pins relative to the delaminated areas.

4.2. Mode-ratio change

The outcome of the fractographic investigation suggests a shift in mode-ratio, as the crack progresses along the span of the laminate. In [19], a trend was identified where the observed fractographic features indicated that the mode-ratio tended to reduce slightly, i.e. change from more Mode II to mixed-mode fracture, as the crack propagated from the root to the tip.

Micrographs of failed Z-pins from two regions, *C2* and *C4*, on the pinned *3R* plate C are shown in Fig. 21. While the failed pins in both regions have failed in shear, the image of region *C2* – closer to the root – indicates a very high Mode II sliding failure as there is little evidence of any pull-out of the Z-pin. However, the pin from region *C4* – closer to the tip – appears to have pulled out by a small amount, also deforming the surrounding resin pocket to a greater extent. It could be inferred that this is caused by the more mixed-mode nature of the crack further along the span of the laminate. As the crack passes the pins, there will be small amount of forced mode I opening during interaction between the pin and the crack and this may then force the crack into a more mixed-mode state, which is exacerbated each time the crack encounters more pin rows. It has been shown previously [20] how the apparent fracture toughness of *NACF* Z-pins increases substantially when the crack is shifted from pure Mode II to even a small amount of mixed-mode failure, and so this finding is significant. More investigation is needed to further examine this effect.

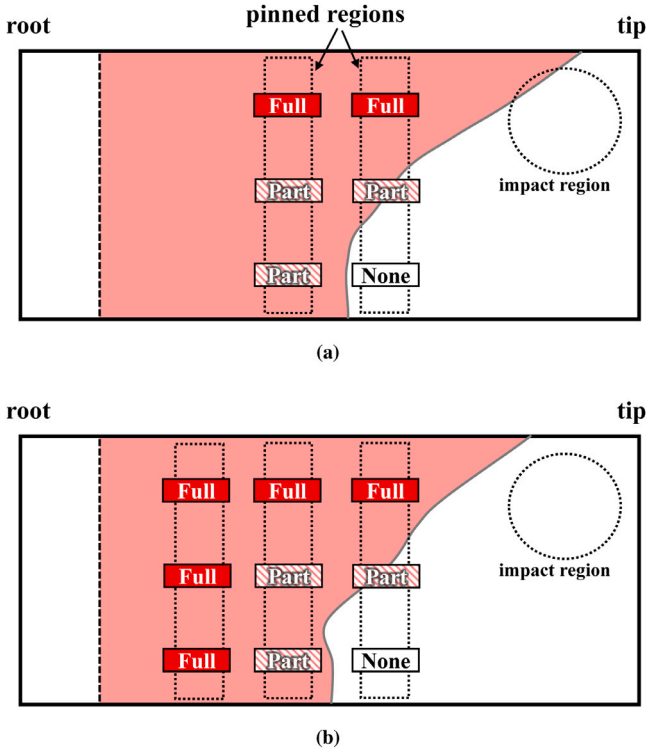

Fig. 20. Fracture surface maps of (a) specimen B (pinned *2R*), and (b) specimen C (pinned *3R*). The overlaid boxes indicate the nature of the pin shear-failure: 'Full' for full rupture, 'Part' for partial failure, and 'None' for no apparent failure.

5. Conclusions

A new high-velocity gelatine impact test design has been used as a test vehicle for investigating the high strain-rate loading behaviour of arrays of normally-aligned carbon fibre (NACF) Z-pins inserted at high density and in generic patterns. The test was designed to achieve a delamination occurring across a large area. The test consists of a tapered, cantilevered impact specimen manufactured from Hexcel IM7/8552 carbon-fibre pre-preg and impacted with ballistic gelatine at a pre-defined impact location, angle and velocity to produce a large, singular delamination near the specimen mid-plane at very high strain-rate.

A series of high-velocity impact tests were conducted on specimens containing 2% areal density arrays of Z-pins in two pre-defined patterns arranged in chordwise 'bands'. The first pattern contained two Z-pin

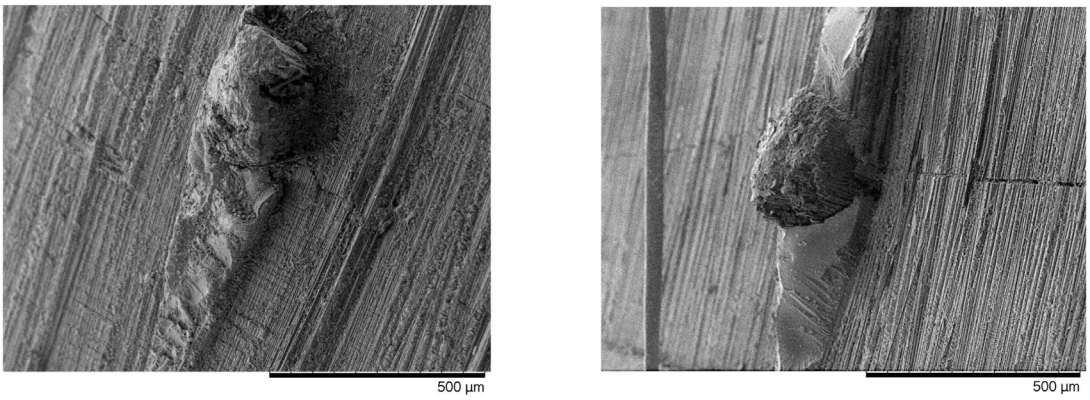

Fig. 21. (a) shows an SEM micrograph of a failed Z-pin from the lower surface of region *C2*, while (b) shows a failed Z-pin from region *C4*.

bands termed '2R' (containing 1,728 Z-pins) and one with three Z-pin bands termed '3R' (containing 2,592 Z-pins). The specimens were tested using a light gas-gun facility and the response recorded using two high-speed video cameras, used to track crack progression and overall specimen impact response in terms of deflections and gelatine behaviour. Ultrasonic C-scanning was performed before and after each test to assess the delamination condition of the specimens. It was shown that inclusion of a third band of pins near the root region where delamination initiates, increasing the number of pins by 50%, has no beneficial effect on arresting the delamination crack. In all cases, the delamination was stopped by the pins and the C-scans showed very similar delamination profiles for all tests (both using 2R and 3R patterns).

An extensive failure investigation was carried out on pinned 2R and pinned 3R laminates to examine the behaviour of the pins during the tests using SEM fractography. Several possible Z-pin energy-dissipating failure mechanisms such as multi-direction ploughing, fibre dragging and fibre gouging were identified. As was the case in [19] for an unpinned laminate, SEM observation of failed Z-pins suggested a possibility that the mode-ratio had changed from pure mode II to mixed-mode as the crack propagated along the span.

CRediT authorship contribution statement

A.D. Cochrane: Investigation, Validation, Formal analysis, Writing – original draft. **J. Serra:** Methodology, Writing – review & editing, Supervision. **J.K. Lander:** Supervision, Conceptualization. **H. Böhm:** Methodology, Investigation. **T. Wollmann:** Methodology, Investigation. **A. Hornig:** Methodology. **M. Gude:** Supervision. **I.K. Partridge:** Supervision, Funding acquisition. **S.R. Hallett:** Conceptualization, Writing – review & editing, Supervision, Funding acquisition.

Declaration of competing interest

The authors declare that they have no known competing financial interests or personal relationships that could have appeared to influence the work reported in this paper.

Acknowledgements

The authors wish to acknowledge the support of Rolls-Royce plc through the Composites University Technology Centre (UTC) at the University of Bristol and through the Lightweight Structures and Materials and Robust Design UTC at the Technische Universität Dresden. The EPSRC, United Kingdom is acknowledged through the Centre for Doctoral Training in Composites Manufacture (grant no. EP/L015102/1) as well as the "Understanding Delamination Suppression at High Deformation Rates in Through-Thickness Reinforced Laminated Composites" project (grant no. EP/M015319/1).

References

[1] Zhu L, Li N, Childs P. Light-weighting in aerospace component and system design. Propuls Power Res 2018;7(2):103–19. http://dx.doi.org/10.1016/j.jppr.2018.04.001.

[2] Zhang X, Hounslow L, Grassi M. Improvement of low-velocity impact and compression-after-impact performance by z-fibre pinning. Compo Sci Technol 2006;66(15):2785–94. http://dx.doi.org/10.1016/j.compscitech.2006.02.029.

[3] Greenhalgh E, Hiley M. The assessment of novel materials and processes for the impact tolerant design of stiffened composite aerospace structures. Composites 2003;34(2):151–61. http://dx.doi.org/10.1016/S1359-835X(02)00188-4.

[4] Cartié DD, Dell'Anno G, Poulin E, Partridge IK. 3D Reinforcement of stiffener-to-skin T-joints by Z-pinning and tufting. Eng Fract Mech 2006;73(16):2532–40. http://dx.doi.org/10.1016/j.engfracmech.2006.06.012.

[5] Dell'Anno G, Treiber J, Partridge I. Manufacturing of composite parts reinforced through-thickness by tufting. Robot Comput-Integr Manuf 2016;37:262–72. http://dx.doi.org/10.1016/j.rcim.2015.04.004.

[6] Pingkarawat K, Mouritz A. Stitched mendable composites: Balancing healing performance against mechanical performance. Compos Struct 2015;123:54–64. http://dx.doi.org/10.1016/j.compstruct.2014.12.034.

[7] Partridge I, Cartie D. Delamination resistant laminates by Z-Fiber® pinning: Part I manufacture and fracture performance. Composites 2005;36(1):55–64. http://dx.doi.org/10.1016/S1359-835X(04)00180-0.

[8] Boyce J, Wallis Jr R, J, Bullock D. Composite structure reinforcement, US Patent 4,808,461. 1989.

[9] Mouritz A. Review of z-pinned composite laminates. Composites 2007;38(12):2383–97. http://dx.doi.org/10.1016/j.compositesa.2007.08.016.

[10] Rugg KL, Cox BN, Massabo R. Mixed-mode delamination of polymer composite laminates reinforced through the thickness by Z-fibers. Composites 2002;33:177–90.

[11] Cui H, Yasaee M, Kalwak G, Pellegrino A, Partridge IK, Hallett SR, Allegri G, Petrinic N. Bridging mechanisms of through-thickness reinforcement in dynamic mode I&II delamination. Composites 2017;99:198–207. http://dx.doi.org/10.1016/j.compositesa.2017.04.009.

[12] Cui H, Yasaee M, Hallett SR, Partridge IK, Allegri G, Petrinic N. Dynamic bridging mechanisms of through-thickness reinforced composite laminates in mixed mode delamination. Composites 2018;106:24–33. http://dx.doi.org/10.1016/j.compositesa.2017.11.017.

[13] Liu H, Yan W, Yu X, Mai Y. Experimental study on effect of loading rate on mode I delamination of z-pin reinforced laminates. Compos Sci Technol 2007;67(7–8):1294–301. http://dx.doi.org/10.1016/j.compscitech.2006.10.001.

[14] Yasaee M, Mohamed G, Pellegrino A, Petrinic N, Hallett SR. Strain rate dependence of mode II delamination resistance in through thickness reinforced laminated composites. Int J Impact Eng 2017;107:1–11. http://dx.doi.org/10.1016/j.ijimpeng.2017.05.003.

[15] Rezai A, Cartia D, Partridge I, Irving P. Interlaminar damage resistance of Z-fiber reinforced structural CFRP, in: Proceedings Of The 13th European Conference On Composite Materials, Beijing, China, 2001.

[16] Yasaee AM, Mohamed BG, Allegri CG, Hallett DSR. Delamination resistance of through-thickness reinforced composites, in: Proceedings Of The 16th European Conference On Composite Materials, Seville, Spain, 2014.

[17] Isa M, Feih S, Mouritz A. Compression fatigue properties of z-pinned quasi-isotropic carbon/epoxy laminate with barely visible impact damage. Compos Struct 2011;93(9):2269–76. http://dx.doi.org/10.1016/j.compstruct.2011.03.015.

[18] Kalwak G, Read S, Jevons M, Petrinic N. Investigation of the delamination characteristics of composite specimens with through-thickness reinforcement using an inertia-constrained soft-body beam bend test specimen, in: Proceedings Of The 16th European Conference On Composite Materials, Seville, Spain, 2014.

[19] Cochrane AD, Serra J, Lander JK, Partridge IK, Böhm H, Wollmann T, Hornig A, Gude M, Hallett SR. Experimental investigation of large-scale high-velocity soft-body impact. Int J Impact Eng 2021;104089. http://dx.doi.org/10.1016/j.ijimpeng.2021.104089.

[20] Yasaee M, Lander J, Allegri G, Hallett S. Experimental characterisation of mixed mode traction–displacement relationships for a single carbon composite Z-pin. Compos Sci Technol 2014;94:123–31. http://dx.doi.org/10.1016/j.compscitech.2014.02.001.

[21] M'membe B, Gannon S, Yasaee M, Hallett SR, Partridge IK. Mode II delamination resistance of composites reinforced with inclined Z-pins. Mater Des 2016;94:565–72. http://dx.doi.org/10.1016/j.matdes.2016.01.051.

[22] Material Data Sheet: Hexply 8552 Data Sheet (EU), Hexcel Corporation, 2016, https://www.hexcel.com/user_area/content_media/raw/HexPly_8552_eu_DataSheet.pdf.

[23] Cartié DD, Troulis M, Partridge IK. Delamination of Z-pinned carbon fibre reinforced laminates. Compos Sci Technol 2006;66(6):855–61. http://dx.doi.org/10.1016/j.compscitech.2004.12.018.